MicroRNA-7/NF-κB signaling regulatory feedback circuit regulates gastric carcinogenesis

Xiao-Di Zhao,[1]* Yuan-Yuan Lu,[1]* Hao Guo,[1]* Hua-Hong Xie,[1] Li-Jie He,[1,2] Gao-Fei Shen,[1] Jin-Feng Zhou,[1] Ting Li,[1] Si-Jun Hu,[1] Lin Zhou,[1] Ya-Nan Han,[1] Shu-Li Liang,[1] Xin Wang,[1] Kai-Chun Wu,[1] Yong-Quan Shi,[1] Yong-Zhan Nie,[1] and Dai-Ming Fan[1]

[1]State Key Laboratory of Cancer Biology, Xijing Hospital of Digestive Diseases and [2]Department of Nephrology, Xijing Hospital, The Fourth Military Medical University, Xi'an, Shaanxi 710032, China

MicroRNAs play essential roles in gene expression regulation during carcinogenesis. Here, we investigated the role of miR-7 and the mechanism by which it is dysregulated in gastric cancer (GC). We used genome-wide screenings and identified *RELA* and *FOS* as novel targets of miR-7. Overexpression of miR-7 repressed RELA and FOS expression and prevented GC cell proliferation and tumorigenesis. These effects were clinically relevant, as low miR-7 expression was correlated with high RELA and FOS expression and poor survival in GC patients. Intriguingly, we found that miR-7 indirectly regulated RELA activation by targeting the IκB kinase IKKε. Furthermore, IKKε and RELA can repress miR-7 transcription, which forms a feedback circuit between miR-7 and nuclear factor κB (NF-κB) signaling. Additionally, we demonstrate that down-regulation of miR-7 may occur as a result of the aberrant activation of NF-κB signaling by *Helicobacter pylori* infection. These findings suggest that miR-7 may serve as an important regulator in GC development and progression.

Introduction

Gastric cancer (GC), despite its general declining incidence, remains the fourth most common cancer and the third leading cause of cancer-related death worldwide (Cancer Genome Atlas Research Network, 2014; Siegel et al., 2014). The evolution of GC has been characterized as progressing through a multistep process whereby cells acquire a series of genetic and epigenetic alterations in key growth-regulatory genes that endow them with proliferative and survival advantages. These alterations can occur in a cancer cell–intrinsic fashion or can be provoked by extrinsic signals from the tumor microenvironment (Fearon and Vogelstein, 1990; Correa, 1992; Hanahan and Weinberg, 2011). *Helicobacter pylori* is a gram-negative bacterium that specifically colonizes mammalian gastric epithelium and is considered to be the strongest known risk factor for gastric malignancies. Infection with *H. pylori* and the resulting chronic inflammation is a major step in the initiation and development of GC. Epidemiological studies have determined that the attributable risk for GC conferred by *H. pylori* is ∼75% (Herrera and Parsonnet, 2009; Polk and Peek, 2010). In addition to causing general inflammatory stress, *H. pylori* infection activates multiple critical pathways in gastric epithelial cells, including nuclear factor κB (NF-κB) and activator protein 1 (AP-1) signaling pathways (Ding et al., 2010). Sustained and constitutive activation of NF-κB and AP-1 transcription factors (TFs) affects various cellular functions, leading to increased inflammatory cytokine production, altered epithelial cell proliferation, and apoptosis rate, finally resulting in epithelial cell oncogenic transformation (Eferl and Wagner, 2003; Quante et al., 2013). Physiologically, cells can use several mechanisms to turn off those activated TFs to avoid prolonged and detrimental inflammatory responses (Ruland, 2011); however, such responses are seemingly overcome during the progression toward carcinogenesis, and the underlying regulatory mechanisms have yet to be fully explored.

miRNAs are a class of small noncoding RNA that post-transcriptionally regulate gene expression through binding to the 3′-UTR of target mRNAs. The effect of these interactions elicits either the inhibition of the translation of the targeted mRNAs and/or their degradation (Bartel, 2004). The functions of miRNAs have been found to extend to both physiological and pathological conditions, including cancer. In human cancer, miRNAs regulate the expression of important cancer-related genes and thereby function as oncogenes or tumor suppressor genes (Esquela-Kerscher and Slack, 2006). Among them, miR-7 has recently been found to be down-regulated and plays

*X.-D. Zhao, Y.-Y. Lu, and H. Guo contributed equally to this paper.

Correspondence to Dai-Ming Fan: daimingfan@fmmu.edu.cn; Yong-Zhan Nie: yongznie@fmmu.edu.cn; or Yong-Quan Shi: shiyquan@fmmu.edu.cn

Abbreviations used in this paper: AP-1, activator protein 1; ChIP, chromatin immunoprecipitation; DIG, digoxigenin; GC, gastric cancer; IHC, immunohistochemistry; IKK, IκB kinase; ISH, in situ hybridization; NF-κB, nuclear factor κB; SI, staining index; TF, transcription factor.

The Rockefeller University Press $30.00
J. Cell Biol. Vol. 210 No. 4 613–627
www.jcb.org/cgi/doi/10.1083/jcb.201501073

a tumor suppressor role in several gastrointestinal cancer types through targeting different oncogenes (Fang et al., 2012; Zhang et al., 2013, 2014; Li et al., 2014; Ma et al., 2014). Our previous study also indicated that miR-7 inhibits metastatic GC cells undergoing epithelial–mesenchymal transition through the miR-7–IGF1R–Snail pathway (Zhao et al., 2013). However, the potential roles of miR-7 in gastric carcinogenesis remain largely unknown. Given that one specific miRNA is capable of targeting multiple genes, it is of particular interest to identify novel miR-7 targets that are causally involved in gastric carcinogenesis. In addition, as an important class of regulatory RNAs, miRNAs themselves are regulated (Siomi and Siomi, 2010). Kong et al. (2012) reported that miR-7 expression in GC specimens was inversely correlated with the levels of certain cytokines, indicating that miR-7 down-regulation is related to the host inflammatory responses. However, the underlying mechanisms by which inflammation contributes to the dysregulation of miR-7 remain to be investigated.

In this study, we used an integrated approach and identified *RELA* and *FOS* as important targets of miR-7 in GC. We systematically validated the tumor-suppressive role of miR-7 by repressing RELA and FOS in a series of experiments performed in in vitro and in vivo models. In addition, we discovered a novel miR-7/IKKε/RELA reciprocal feedback loop, whose perturbation may promote the initiation and development of GC induced by *H. pylori* infection.

Results

Identification of miR-7 targets by the combination of proteomic and transcriptomic profiling

To gain insight into the overall miR-7–regulated genes in GC, we combined the proteomic and transcriptomic approaches to identify novel targets of miR-7. For that purpose, we transfected BGC823 cells with miR-7 mimics and negative controls. Increased expression of miR-7 upon transfection was confirmed by real-time PCR (Fig. S1). We used an iTRAQ-based quantitative proteomic approach to search for putative miR-7 targets. Equal amounts of protein lysates from cells transfected with miR-7 and controls were used for iTRAQ analysis as outlined in Fig. 1 A. In addition, we performed a cDNA microarray to examine the effects of miR-7 on BGC823 transcriptome. We found that miR-7 overexpression resulted in considerable changes in gene expression at the mRNA and protein levels (Fig. 1 B). Of the 3,129 common proteins quantified by iTRAQ in two biological replicates, 1,377 protein abundance values were cross-referenced with microarray data. We observed a Spearman rank correlation of 0.47 between protein and mRNA abundance for these genes (Fig. 1 C). Using twofold as a cut-off to designate differentially expressed genes, we found 180 genes that were down-regulated at the mRNA level, 75 genes that were down-regulated at the protein level, and 39 down-regulated genes that overlapped at both mRNA and protein levels in BGC823 cells after miR-7 overexpression (Fig. 1 D and Tables S1, S2, S3, S4, and S5). We used three bioinformatic algorithms and found that 16 out of the 39 genes contain miR-7 binding sites (Table S3). Among them, *RELA* is a prominent member of the NF-κB TF family; we also noticed that *FOS*, a key component of AP-1, was significantly down-regulated at the mRNA level and carried three potential miR-7 target sites (Table S1). These data, along with the notion that both NF-κB and AP-1 are critical TFs that orchestrate the expression of many genes involved in cell proliferation and survival, led to the hypothesis that *RELA* and *FOS* might be important targets of miR-7 during gastric carcinogenesis.

miR-7 directly targets RELA and FOS 3′-UTRs

To verify whether *RELA* and *FOS* are direct targets of miR-7, we performed luciferase reporter assays in BGC823 cells. *RELA* and *FOS* 3′-UTRs containing the miR-7 binding sites and their mutant counterparts were cloned downstream of the luciferase open reading frame (Fig. 2 A). miR-7 overexpression suppressed luciferase activities of the *RELA* and *FOS* 3′-UTR reporter constructs, whereas the effect was abolished when two and three mutations were introduced into their seed sequences, respectively (Figs. 2 B and S2 A). Moreover, the mRNA and protein levels of *RELA* and *FOS* were substantially decreased after the ectopic expression of miR-7 in BGC823 and SGC7901 cells, as indicated by real-time PCR and Western blotting. Conversely, knockdown of miR-7 increased the mRNA and protein levels of *RELA* and *FOS* (Fig. 2, C and D; and Fig. S2 B). These results supported our high-throughput screening results and demonstrated *RELA* and *FOS* as direct targets of miR-7 in GC cells.

miR-7 expression and its correlation with clinicopathological characteristics of GC patients

Having noted that miR-7 down-regulates *RELA* and *FOS* expression in GC cells, we investigated whether the regulation also occurs in vivo. We first investigated the expression of miR-7, *RELA*, and *FOS* in freshly collected GC samples. We observed that almost all of the GC samples exhibited a down-regulation of miR-7 and up-regulation of RELA and FOS compared with their adjacent normal tissues (Fig. 3, A and C) and an inverse correlation between miR-7 and RELA or FOS (Fig. 3 D). Moreover, we examined miR-7 expression by in situ hybridization (ISH) analysis in a cohort of 106 GC samples, followed by immunohistochemistry (IHC) staining for RELA and FOS. As shown in Fig. 3 E, GC with low miR-7 expression exhibited a more malignant phenotype, whereas GC with high miR-7 expression exhibited more epithelial-like characteristics with the formation of gland-like tubular structures. Consistently, an inverse expression pattern between miR-7 and RELA or FOS was also observed (Fig. 3 F). Furthermore, correlation analysis showed that low miR-7 expression was significantly associated with a more aggressive phenotype in GC (Table 1). Kaplan-Meier analysis revealed that low miR-7 expression was associated with shorter disease-free survival (Fig. 3 G). Cox regression analysis indicated that low miR-7 expression was an independent prognostic factor for poor survival in GC patients (Table 2).

Suppression of RELA and FOS is functionally important for the biological effects of miR-7

To confirm the expression of miR-7 in GC cells, real-time PCR analysis for miR-7 as well as another two previously reported dysregulated miRNAs (miR-21 and let-7a; Song and Ajani, 2013) was performed in BGC823 and SGC7901 cells, and the results were compared with that of GES cells, an immortalized gastric epithelial cell line (Fig. S3 A). To elucidate the biolog-

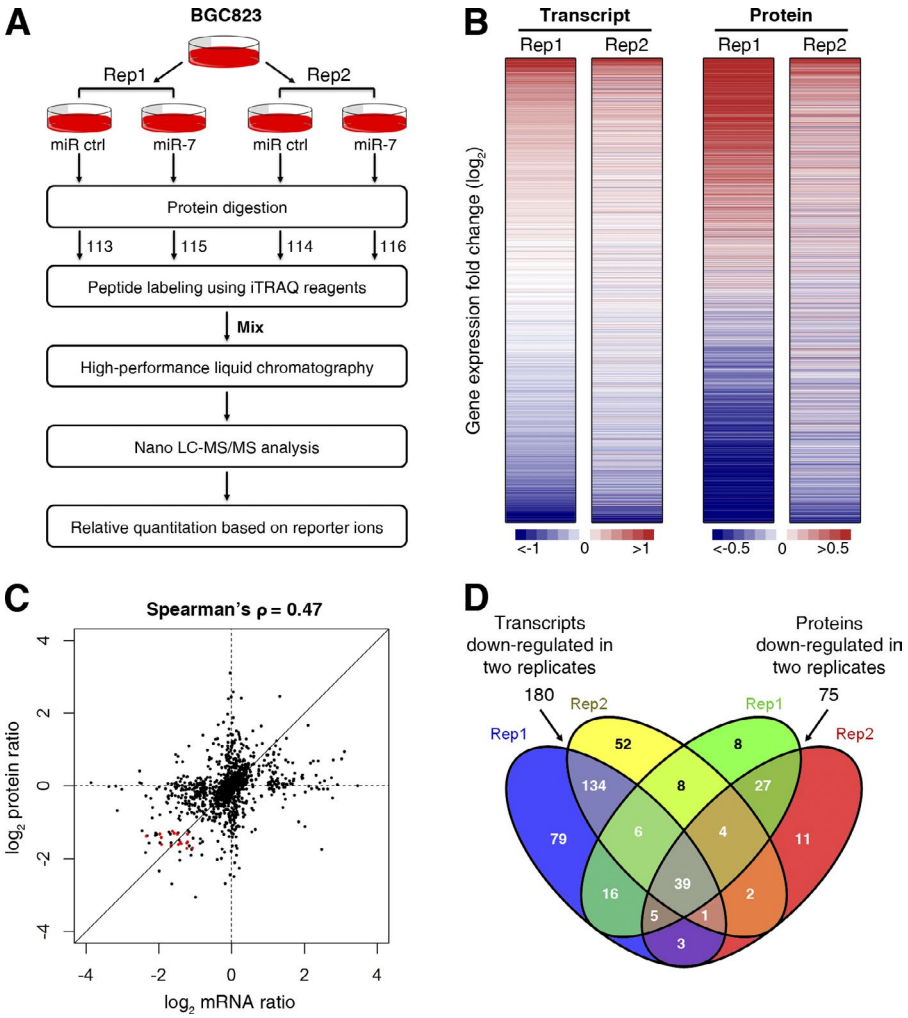

Figure 1. **Proteomic and transcriptomic identification of miR-7 targets.** (A) Workflow for the identification of differentially expressed proteins between miR-7 mimic (miR-7)–transfected and miRNA mimic negative control (miR ctrl)–transfected BGC823 cells. 113, 115, 114, and 116 indicate the iTRAQ reporter ions. LC-MS/MS, liquid chromatography coupled to tandem mass spectrometry. (B) Heat maps depict the relative expression of all transcripts (n = 13,400) and proteins (replicate 1, n = 5,184; replicate 2, n = 4,303) in BGC823 cells after miR-7 overexpression compared with control cells. Intensities are normalized for each gene in each row. Values express the $\log_2$ transformed fold change. (C) Protein abundance compared with mRNA abundance, relative to control cells, for 1,377 genes in BGC823 cells. Genes containing miR-7 target sites (red dots) in their 3′-UTR exhibited significantly reduced expression at both mRNA and protein levels. (D) Overlap between differentially expressed ($\log_2$-fold change less than −1) transcripts and proteins identified in the fourplex experiment. The data shown are from two sets of biological replicates.

ical significance of miR-7 in gastric carcinogenesis, we examined the effects of miR-7 on proliferation and clonogenicity in BGC823 and SGC7901 cells. We observed that the overexpression of miR-7 reduced the proliferation rate and caused G0/G1 arrest in both BGC823 and SGC7901 cells (Fig. 4 A). The ability of miR-7 to inhibit cell proliferation was further confirmed by colony formation assays in BGC823 cells (Fig. 4 B). Soft agar colony formation assays indicated that miR-7 also reduced the ability of GC cells to grow in an anchorage-independent manner (Fig. 4 C). In contrast, the inhibition of miR-7 accelerated GC cell growth and cell cycle progression (Fig. 4, A–C). Furthermore, the overexpression of miR-7 increased, whereas the inhibition of miR-7 decreased, the percentage of early apoptotic cells in SGC7901 and BGC823 cells compared with control cells (Fig. 4 D). In addition, the overexpression of miR-7 sensitized the multi-drug–resistant GC cell line SGC7901/VCR to the chemotherapeutic agents cisplatin and 5-fluorouracil, whereas the inhibition of miR-7 rendered the cells more resistant to these treatments (Fig. 4 D). We next tested whether RELA and FOS represent miR-7 mediators whose dysregulation is required for GC cell growth. We used siRNAs to knock down RELA and FOS in GC cells (Fig. S3 B). Similar to what was observed upon miR-7 overexpression, RELA and/or FOS silencing impaired GC cell proliferation (Fig. 4 E). We further investigated whether the reduced proliferation induced by miR-7 was mainly mediated by targeting RELA and FOS. We constructed RELA- and FOS-expressing plasmids containing wild-type or mutant miR-7 binding sites in their 3′-UTRs and transfected them into SGC7901 and BGC823 cells (Fig. S3 C). As expected, the ectopic expression of RELA or FOS with mutant 3′-UTR rescued the function of RELA and FOS and exhibited a stronger proliferation potential than the expression of the wild-type gene when cotransfected with miR-7 (Figs. 4 F and S3 D). Collectively, these results demonstrate that miR-7 plays an important role in inhibiting the tumorigenicity of GC cells and that RELA and FOS are important mediators of miR-7's effects.

miR-7 suppresses the tumor growth of the GC cell xenograft in nude mice

To explore the relationship between miR-7 and tumorigenesis in vivo, the xenograft model of GC cells in nude mice was adopted. We used lentiviral vectors for the stable expression of miR-7 (LV-miR-7) and miR-7 inhibitor (LV-anti-7) in BGC823 cells. The expression of mature miR-7 (miR-7-5p) was confirmed by real-time PCR (Fig. S4 A). BGC823 cells that stably expressed LV-miR-7, LV-anti-7, or their controls were injected subcutaneously into each flank of nude mice. The tumor volumes were monitored, and the growth curves of the tumors were plotted accordingly. We found that miR-7 overexpression significantly decreased tumor growth and the inhibition of miR-7 promoted tumor growth in vivo (Fig. 5, A–C). We further performed IHC staining for Ki67, PCNA, RELA, and FOS in the

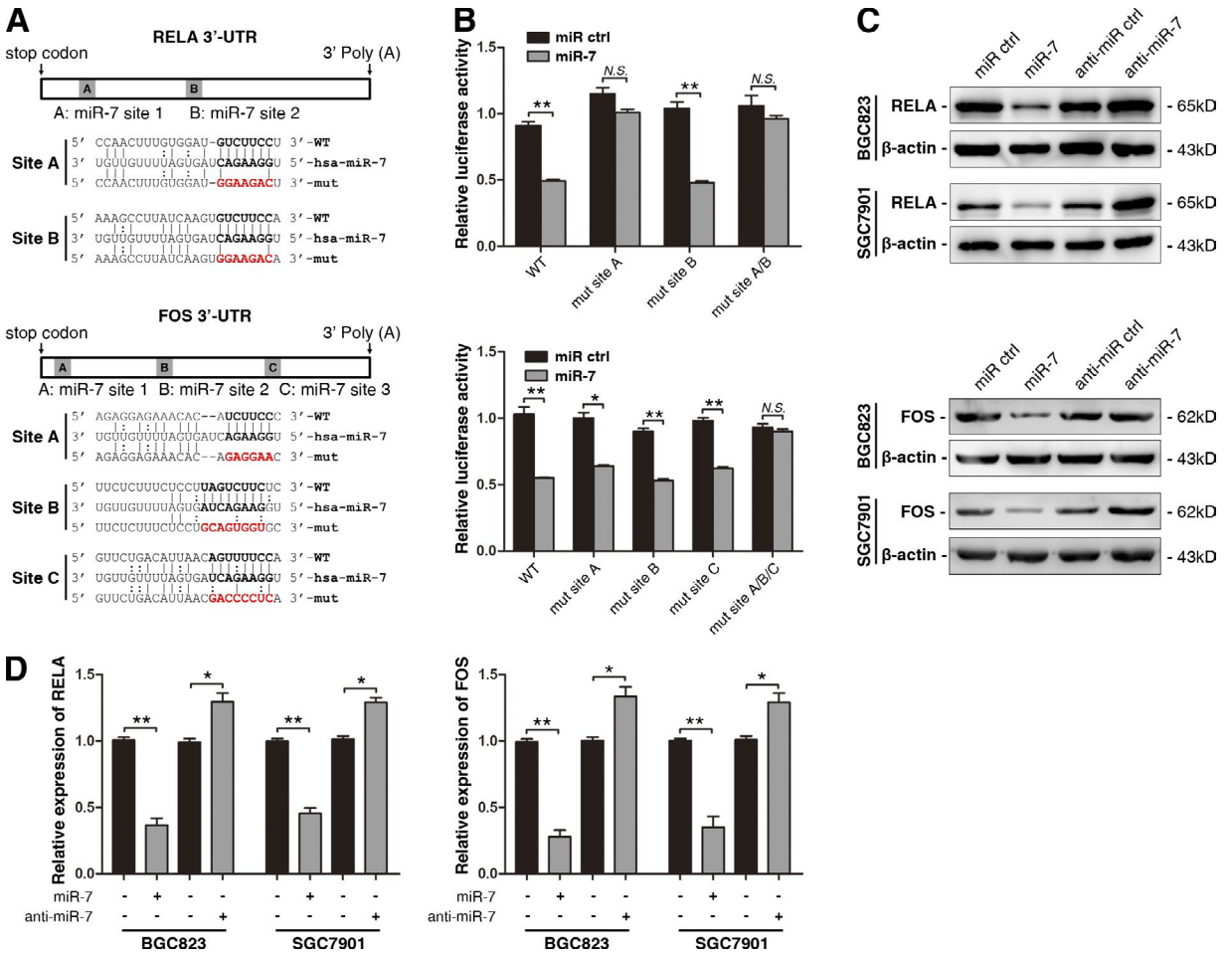

Figure 2. **miR-7 directly targets RELA and FOS.** (A) Predicted duplex sequences between wild-type (WT) or mutant (mut) *RELA* and *FOS* 3′-UTRs and miR-7. The red and bold portions of the sequences represent the mutant miR-7 binding sites in *RELA* and *FOS* 3′-UTRs. (B) Luciferase activity derived from the indicated 3′-UTR reporter constructs after cotransfection into BGC823 cells with miR-7 mimic (miR-7)–transfected and miRNA mimic negative control (miR ctrl)–transfected BGC823 cells. (C and D) Western blot (C) and real-time PCR (D) analysis of RELA and FOS protein and mRNA levels after the transfection of miR-7, miR-7 inhibitor (anti–miR-7), or their negative controls (miR ctrl and anti-miR ctrl) in BGC823 and SGC7901 cells. Histograms show the means ± SD (error bars) of three experiments performed in triplicates. *, $P < 0.05$; **, $P < 0.01$; *N.S.*, not significant ($P > 0.05$).

tumors. Compared with the negative control, miR-7 overexpression significantly suppressed proliferative activity, as indicated by the percentage of cells positive for Ki67 and PCNA staining, and inhibited RELA and FOS protein expression. In contrast, miR-7 inhibition increased the percentages of Ki67- and PCNA-positive cells and the levels of RELA and FOS expression (Fig. 5 D). We extracted the proteins from the tumors and examined the protein expressions of RELA, FOS, PCNA, and cyclin D1 by Western blot. The results show that miR-7 overexpression significantly inhibited the expression of these proteins, but miR-7 inhibition increased the levels of these proteins (Fig. S4 B). These in vivo observations confirmed the key role of miR-7 in the control of GC cell growth and may serve as a potential therapeutic target for GC treatment.

miR-7 regulates RELA activation by modulating IKKε

Accumulated evidence indicates that cancers associated with chronic inflammation are frequently dependent on aberrant NF-κB activity (Karin and Greten, 2005); we therefore sought to determine whether miR-7 counteracts the NF-κB activity in response to inflammatory stimuli in gastric cells. We observed that the inhibition of miR-7 increased RELA protein levels and the overexpression of miR-7 attenuated lipopolysaccharide-induced RELA activation in GES cells (Figs. 6 A and S4 C). Interestingly, the manipulation of miR-7 expression not only reduced total RELA levels but remarkably changed RELA phosphorylation (p-RELA). We investigated whether the change in p-RELA is exclusively caused by the inhibitory effect of miR-7 on total RELA protein level or whether any other upstream regulatory elements are involved. We examined the expression of IκBα, a major inhibitor of NF-κB, and found that miR-7 overexpression decreased IκBα but increased the phosphorylation of IκBα (p-IκBα), indicating that the degradation of IκBα was involved in the miR-7–mediated regulation of RELA. The degradation of IκBα depends on the phosphorylation of the IκB kinase (IKK) complex, which contains IKKα, IKKβ, IKKε, and TBK1 (Clément et al., 2008). Analyzing their 3′-UTRs revealed that *CHUK* (encoding IKKα) and *IKBKE* (encoding IKKε) contain a putative binding site for miR-7 (Fig. 6 B). We found that miR-7 overexpression or inhibition affected the protein levels of IKKε but not IKKα in both GES and BGC823 cells (Figs. 6 C and S4 D). Luciferase reporter assays further demonstrated that

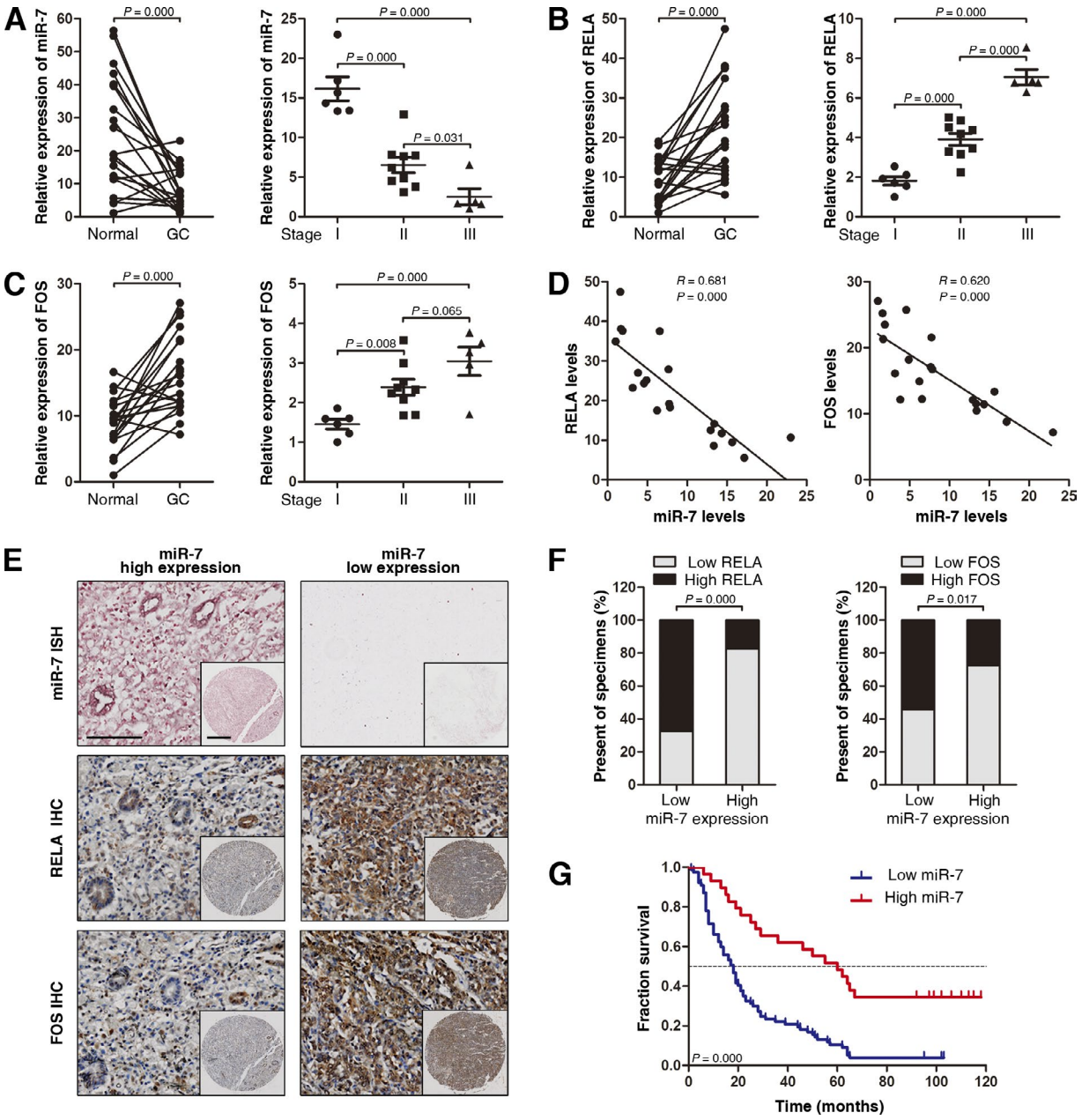

Figure 3. **Clinical relevance of miR-7 and expression of its targets in GC.** (A–C) Real-time PCR analysis of miR-7 (A), *RELA* (B), and *FOS* (C) expression levels from 20 freshly collected GC and their adjacent normal tissues (left). Analysis of the miR-7, *RELA*, and *FOS* expression levels from the 20 paired gastric tissues according to their tumor stage (right). (D) Correlation between miR-7 expression and *RELA* and *FOS* expression in the clinical samples described. (E) Representative images of ISH staining for miR-7 and IHC staining for RELA and FOS in low and high miR-7 expression GC cases. Bars: (main) 100 µm; (inset) 500 µm. (F) The association between miR-7 expression and RELA and FOS levels in GC specimens. (G) Kaplan-Meier overall survival curves for GC patients with low and high expression of miR-7. The low and high expression levels of miR-7 were evaluated semi-quantitatively by staining intensity (low, no or weak staining; high, moderate or intense staining).

miR-7 directly targets the *IKBKE* 3′-UTR (Fig. 6 D). However, *IKBKE* mRNA was unaffected by the overexpression or inhibition of miR-7 (Fig. S4 E). Furthermore, we transfected GES cells with an IKKε construct containing a wild-type or mutant 3′-UTR and treated them with miR-7 mimics. We found that the overexpression of IKKε with a mutant 3′-UTR partly restored both phosphorylated and total forms of RELA in the context of miR-7 overexpression (Figs. 6 E and S4 F). These findings demonstrated that IKKε is involved in the miR-7–mediated modulation of RELA activation.

miR-7 and NF-κB signaling forms a double-negative feedback loop in GC cells

A previous study reported that miR-7 expression was inversely correlated with interleukin-1β and tumor necrosis factor α levels in GC samples (Kong et al., 2012). Because both of these cytokines can induce NF-κB activation (Li and Verma, 2002), we suspected that NF-κB signaling may regulate miR-7 expression. Consistent with this conjecture, the ectopic expression of IKKε or RELA in GES cells reduced the expression of the primary transcript (pri-miR-7) and mature miR-7. Conversely, BGC823

Table 1. **Correlation of miR-7 expression in 106 cases of GC tissue with patients' clinicopathological variables**

Variables	miR-7 expression			P-value
	All cases *n* = 106	Low expression *n* = 67	High expression *n* = 39	
Gender				0.652
Male	67	50	17	
Female	39	27	12	
Age (years)				0.515
≤57.1[a]	55	38	16	
>57.1	51	39	12	
Tumor size (cm)				0.002
≤5	51	30	21	
>5	55	47	8	
Grade of differentiation				0.007
Grade 1	6	1	5	
Grade 2	46	35	11	
Grade 3	54	41	13	
TNM stage[b]				0.000
I	13	2	11	
II	17	7	10	
III	66	60	6	
IV	7	7	0	

[a]Mean age at operation.
[b]Three cases with missing values.

cells treated with IKKε or RELA siRNA led to increased pri-miR-7 and mature miR-7 expression (Fig. 7 A and Fig. S5, A and B). These data suggest that NF-κB signaling controls miR-7 expression by regulating its transcription. We analyzed the 2-kb region upstream from the miR-7-1, -2, and -3 precursor coding sequences using the University of California Santa Cruz Genome Browser and identified seven clusters of putative NF-κB binding sites (referred to as A–G) located 1,319, 459, and 185 bp upstream of the miR-7-1 precursor sequence, 1,215 and 719 bp upstream of the miR-7-2 precursor sequence, and 1,774 and 250 bp upstream of the miR-7-3 precursor sequence (Fig. 7 B). Chromatin immunoprecipitation (ChIP) analysis further showed that RELA was bound to the A, B, and E sites in both BGC823 and SGC7901 cells (Fig. 7 B). These findings thus suggested that a double-negative feedback loop may exist between miR-7 and NF-κB signaling. Indeed, IKKε and nuclear RELA were significantly decreased in miR-7–overexpressing cells and increased when miR-7 was suppressed (Fig. 7 C). Furthermore, the ectopic expression of miR-7 significantly attenuated the expression of known NF-κB target genes in both GC cells (Fig. 7 D). These data suggest that miR-7 and IKKε/RELA can reciprocally regulate each other.

Because *H. pylori* stimulation has been shown to induce aberrant NF-κB activation and cause gastric chronic inflammation (Maeda et al., 2000), we hypothesized that the down-regulation of miR-7 by increased NF-κB activity may be attributable to *H. pylori* infection. Indeed, the co-culture of GES cells with *H. pylori* resulted in a pronounced induction of IKKε and RELA, which was accompanied by a repression of miR-7 expression. Furthermore, pretreatment of GES with the NF-κB inhibitor BAY 11–7082 resulted in the down-regulation of IKKε and RELA and the partial inhibition of miR-7 repression (Fig. 7 E and Fig. S5, C and D). Collectively, these results indicate that *H. pylori* infection disrupts this circuit via the induction of IKKε and RELA, which may contribute to the down-regulation of miR-7.

Table 2. **Univariate and multivariate analysis of factors associated with disease-free survival of GC patients**

Variables	Case number[a]	Hazard ratios (95% CI)[b]	P-value
Univariate analysis			
Gender (male vs. female)	67/39	0.88 (0.58–1.34)	0.558
Age (>57.1 vs. ≤57.1)	51/55	1.74 (1.16–2.63)	0.008
Tumor size (>5 vs. ≤5)	55/51	1.77 (1.17–2.67)	0.007
Grade of differentiation (Grade 3 vs. Grade 1/2)	53/52	1.50 (0.99–2.27)	0.053
TNM (I/II vs. III/IV)	73/30	2.93 (1.78–4.83)	0.000
miR-7 (high vs. low)	29/77	2.82 (1.70–4.67)	0.000
Multivariate analysis			
Age (>57.1 vs. ≤57.1)	51/55	1.73 (1.13–2.66)	0.011
Tumor Size (>5 vs. ≤5)	55/51	1.07 (0.68–1.70)	0.770
Grade of differentiation (Grade 3 vs. Grade 1/2)	53/52	1.32 (0.86–2.02)	0.208
TNM (I/II vs. III/IV)	73/30	2.21 (1.26–3.89)	0.006
miR-7 (high vs. low)	29/77	1.93 (1.15–3.24)	0.014

[a]Analysis was conducted on 106 cases shown in Table 1.
[b]Hazard ratios (95% confidence interval [CI]) and p-values were calculated using univariate or multivariate Cox proportional hazard regression.

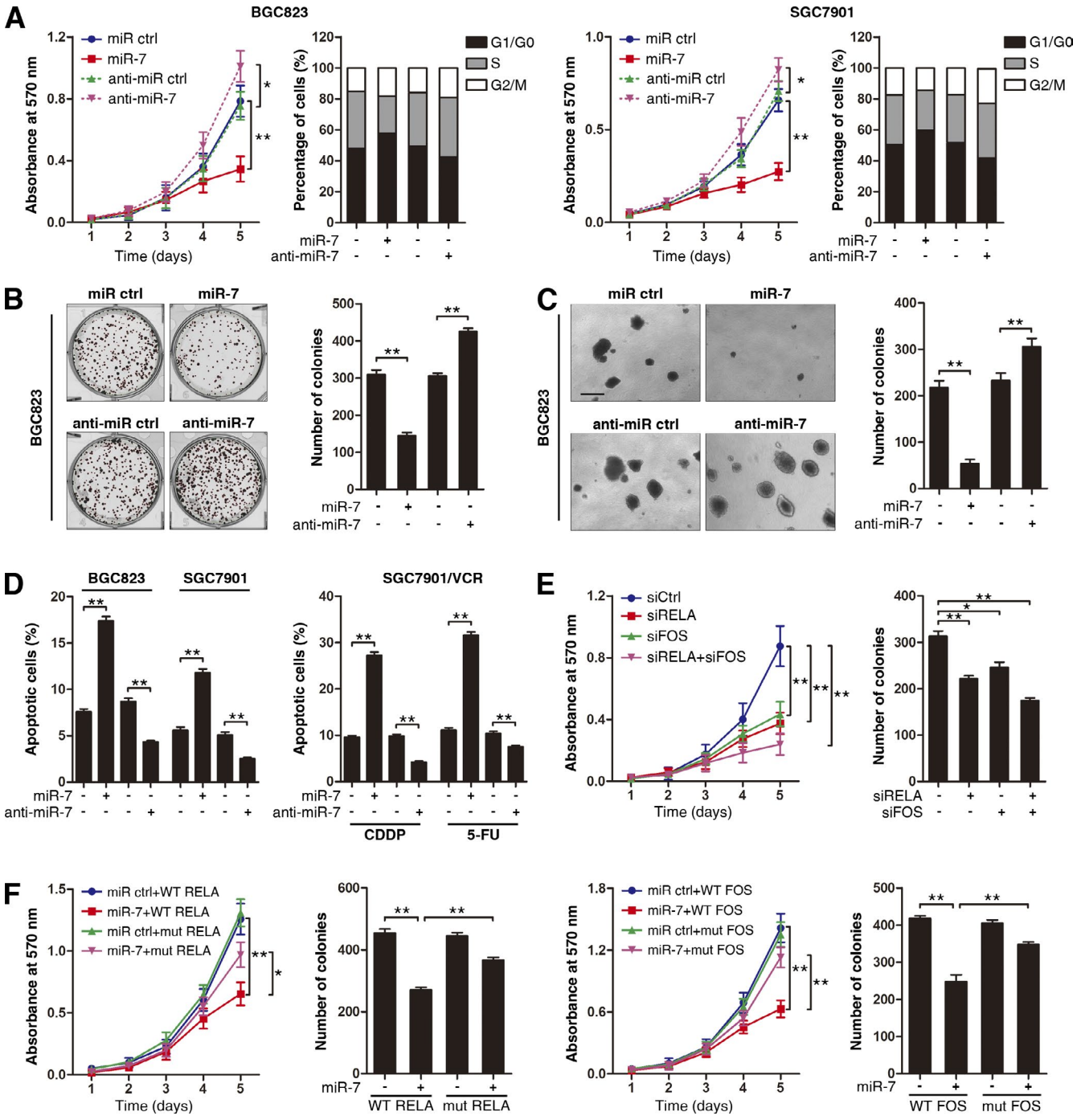

Figure 4. **miR-7 inhibits GC cell proliferation and survival in vitro.** (A) Growth curves and cell cycle analyses of the indicated GC cells transfected with miR-7, anti–miR-7, or their negative controls. Means ± SD (error bars) of a representative experiment (n = 3) performed in triplicates are shown. (B and C) Colony formation (B) and soft agar (C) assays were performed in BGC823 cells transfected with miR-7, anti–miR-7, or their negative controls. Results from a representative experiment (n = 3) performed in triplicates are expressed as the means ± SD. Bar, 500 µm. (D) The apoptotic rate of the indicated cells transfected with miR-7, anti–miR-7, or their negative controls (left) or together with cisplatin (CDDP) and 5-fluorouracil (5-FU) treatment (right). Data are the means ± SD of three independent experiments. (E) Growth curves (left) and colony formation assays (right) of BGC823 cells transfected with RELA siRNA (siRELA), FOS siRNA (siFOS), or control siRNA (siCtrl). Means ± SD of a representative experiment (n = 3) performed in triplicates are shown. (F) Growth curves and colony formation assays of BGC823 cells transfected with RELA (left) or FOS (right) vectors containing wild-type or mutant 3′-UTR and then treated with miR-7 mimic (miR-7)–transfected and miRNA mimic negative control (miR ctrl)–transfected BGC823 cells. Means ± SD of a representative experiment (n = 3) performed in triplicates are shown. *, $P < 0.05$; **, $P < 0.01$.

Discussion

Because each miRNA is estimated to target several hundred distinct genes, their roles are conceivably as important as TFs or signaling molecules in controlling various cellular processes. The functional characterization of an miRNA heavily relies on the identification of its targets and its effects on their expression (He and Hannon, 2004), but most of the newly iden-

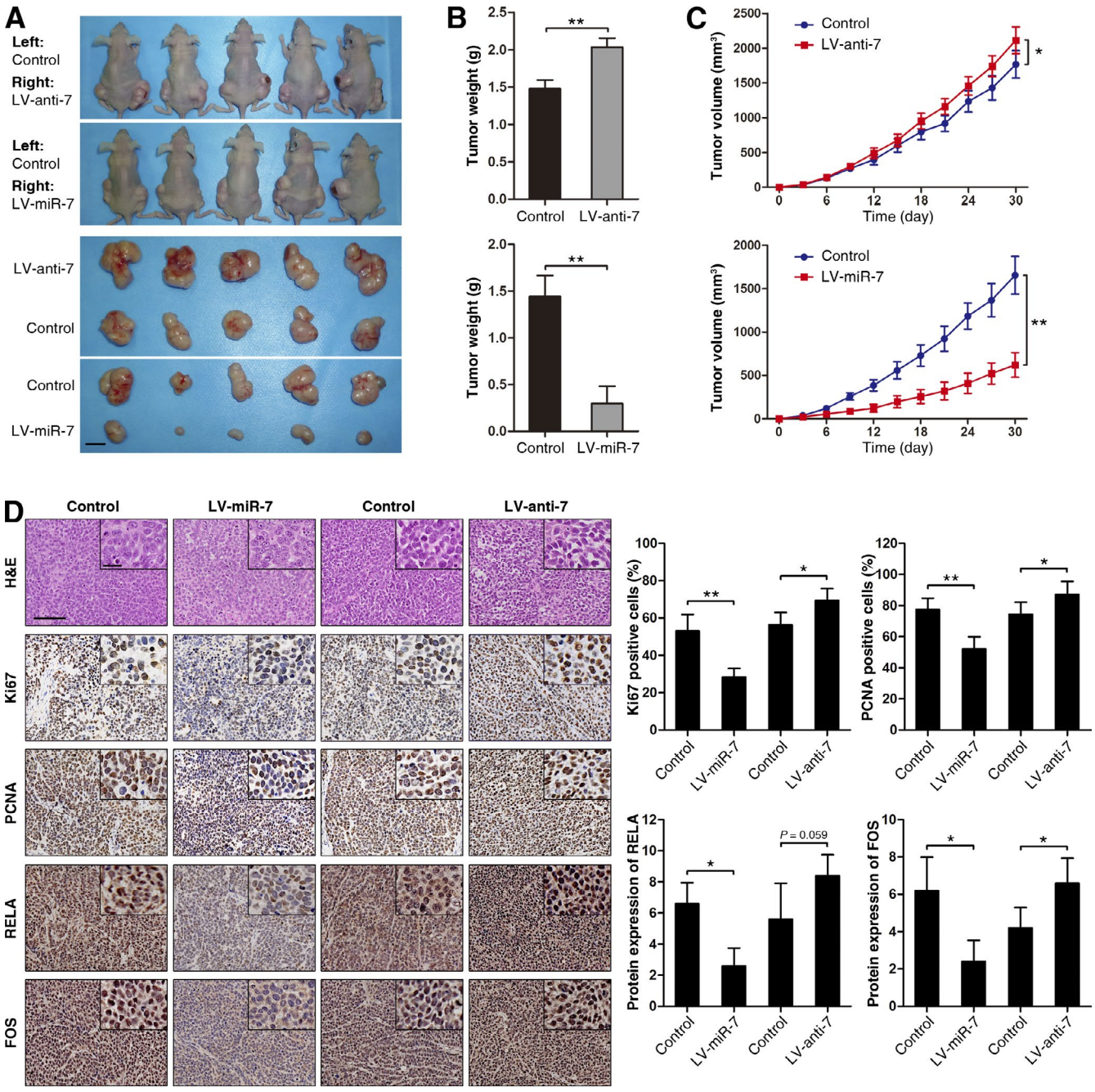

Figure 5. **miR-7 suppresses tumorigenesis in a xenograft model.** (A) Representative image of tumors in nude mice after the injection of BGC823 cells stably expressing LV-miR-7, LV-anti-7, and their controls ($n = 5$). Bar, 1 cm. (B and C) Quantification of tumor weights (B) and growth curves (C) of xenograft tumors in mice. (D, left) Representative images of tumor samples that were stained with hematoxylin and eosin (H&E), Ki67, PCNA, RELA, and FOS by IHC. (right) The percentages of Ki67- and PCNA-positive cells and the levels of RELA and FOS protein expression were measured. Bars: (main) 100 µm; (insets) 25 µm. Error bars show SDs. *, $P < 0.05$; **, $P < 0.01$.

tified mammalian miRNAs have unknown functions. Target identification remains a major challenge because animal miRNAs bind to their targets with partial complementarity over short sequences and the rules of targeting are not completely understood (Thomas et al., 2010). In this study, we combined quantitative iTRAQ experiments, gene expression microarray profiling, and bioinformatic predictions to examine the impact of miR-7 on gene expression and identified *RELA* and *FOS* as important functional targets of miR-7 in GC cells. Typically, bioinformatic algorithms predict hundreds to thousands of targets for each miRNA, but the false-positive rate of these programs is ∼20–70% (Sethupathy et al., 2006). In addition, although high-throughput methods can generate more sensitive and reproducible data, proteomics, as well as transcriptomic studies, cannot distinguish between direct and indirect miRNA targets (Thomas et al., 2010). Therefore, we combined these high-throughput methods with algorithms to filter the candidate gene list by requiring differentially expressed genes with an miRNA binding site. Using this principle, among the genes that were shown to be down-regulated at the mRNA and pro-

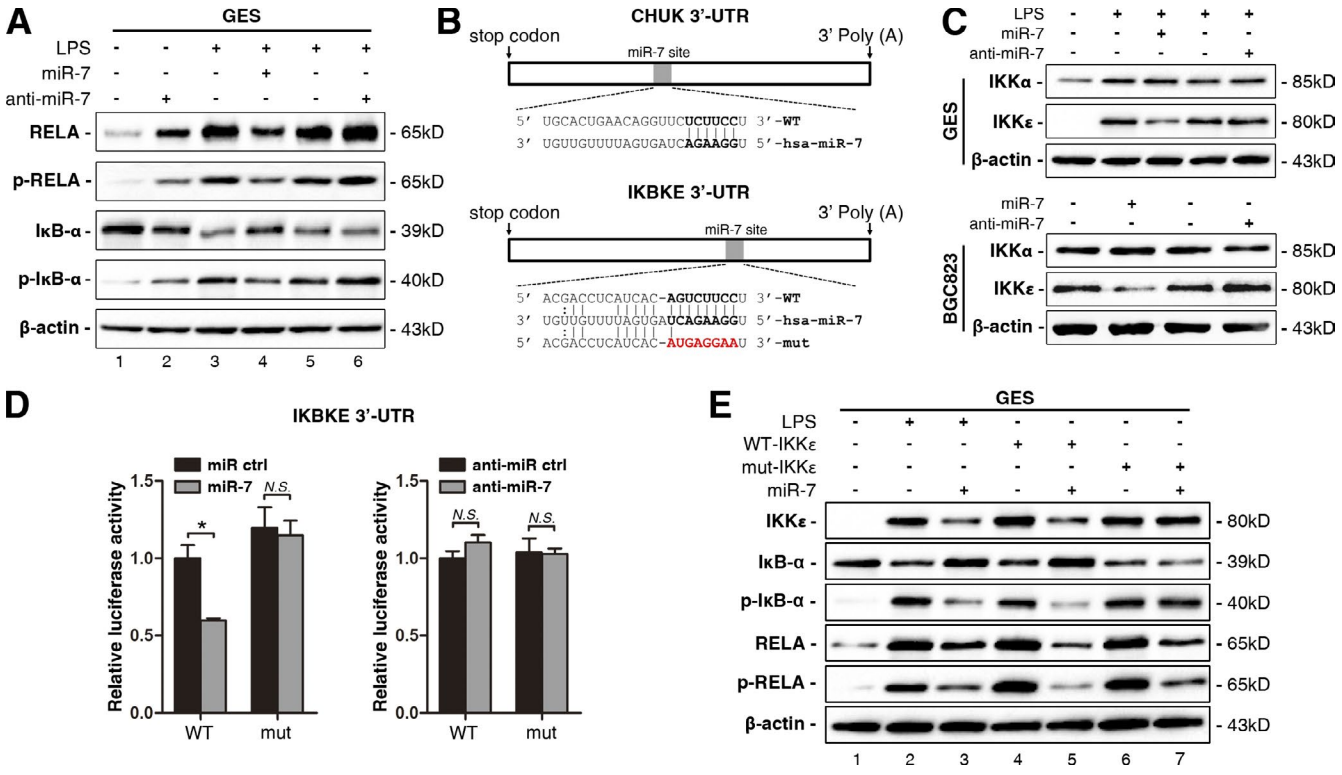

Figure 6. **miR-7 regulates RELA activation by modulating IKKε.** (A) Western blot analysis of RELA, p-RELA, IκBα, and p-IκBα levels in GES cells after the indicated treatment. LPS, lipopolysaccharide. (B) Predicted duplex sequences between *CHUP* and *IKBKE* 3′-UTRs and miR-7. (C) Western blot analysis of IKKα and IKKε levels in the indicated cells after miR-7 overexpression and inhibition. (D) Luciferase activity derived from the indicated 3′-UTR reporter constructs after cotransfection into BGC823 cells with miR-7, anti–miR-7, or their negative controls. Results show the means ± SD (error bars) of three experiments performed in triplicates. (E) The changes in IKKε, IκBα, p-IκBα, RELA, and p-RELA levels in GES cells when cotransfected the IKKε plasmids containing the wild-type or mutant 3′-UTR, along with miR-7 or control, were detected by Western blotting. *, $P < 0.05$; *N.S.*, not significant ($P > 0.05$).

tein levels, *RELA* and *FOS* attracted our attention because they are critical components in NF-κB and AP-1 signaling and carry two and three miR-7 binding sites, respectively. The subsequent luciferase assays and functional validation supported the conclusion that *RELA* and *FOS* are important mediators of miR-7's effects in GC cells. In addition, previously validated miR-7 targets, including *YY1* (Zhang et al., 2013), *IGF1R* (Zhao et al., 2013), *EGFR* (Kefas et al., 2008), and *PIK3R3* (Xu et al., 2013), were among our identified genes. These results suggest that high-throughput screening after miRNA transfection might be an effective tool with which to identify miRNA targets. However, it was noteworthy that both transcriptomic and proteomic screening have systemic strengths and drawbacks. Microarray analysis produces high genomic coverage, but some targets that are repressed at the protein level without being affected at the mRNA level can be missed. Quantitative proteomic methods are thought to be the most direct way of identifying miRNA targets, but current proteomic methodologies are limited and cannot achieve full and comprehensive proteome coverage (Li et al., 2012). Collectively, the optimal approach might involve combining transcriptomic and proteomic analyses for the screening of miRNA targets.

Evidence has shown miRNAs to be novel diagnostic and therapeutic tools, and the primary focus of miRNA research is to understand their functions and underlying molecular mechanisms in cancer. miR-7 has been characterized as a tumor suppressor in various cancers and has been shown to suppress multiple malignant phenotypes including cell proliferation, survival, migration, and invasion (Kalinowski et al., 2014). A series of molecules have been reported as the direct targets of miR-7 in different cell contexts. In glioblastoma, lung, breast, and prostate cancer, and head and neck cancer, miR-7 directly inhibits EGFR expression and downstream AKT and ERK-1/2 activity, which retards tumor growth (Kefas et al., 2008; Webster et al., 2009; Kalinowski et al., 2012). In addition, miR-7 also targets other molecules involved in EGFR signaling, such as RAF (Webster et al., 2009; Rai et al., 2011; Kalinowski et al., 2012), PAK1 (Reddy et al., 2008; Saydam et al., 2011), IRS-1/2 (Kefas et al., 2008; Reddy et al., 2008; Giles et al., 2013), PIK3CD, and mTOR (Fang et al., 2012), in various cancer cell types, suggesting coordinated regulation of the EGFR pathway. Besides the EGFR pathway, miR-7 also targets IGF1R in GC (Zhao et al., 2013) and downstream IRS-2 and PAK1 in tongue squamous cell carcinoma (Jiang et al., 2010). In addition, miR-7 has also been reported to target cell cycle– and apoptosis-related genes such as CCNE1 (Zhang et al., 2014), BCL-2 (Xiong et al., 2011), and XIAP (Liu et al., 2013) in liver, lung, and cervical cancer. Despite a significant amount of evidence supporting a tumor-suppressive role for miR-7, the opposite effect has also been reported (Chou et al., 2010; Yu et al., 2013). These conflicting findings imply that the ambiguous role of miR-7 in regulating the complex network of oncogenes and tumor suppressors in different tumor types requires further exploration. In the present study, we investigated the role of miR-7 in human GC cells and provide several lines of evidence that support miR-7 function as a tumor suppressor. First, we used two distinct human GC cell lines as models; in vitro gain- and loss-of-function experiments demonstrated that miR-7 overexpression

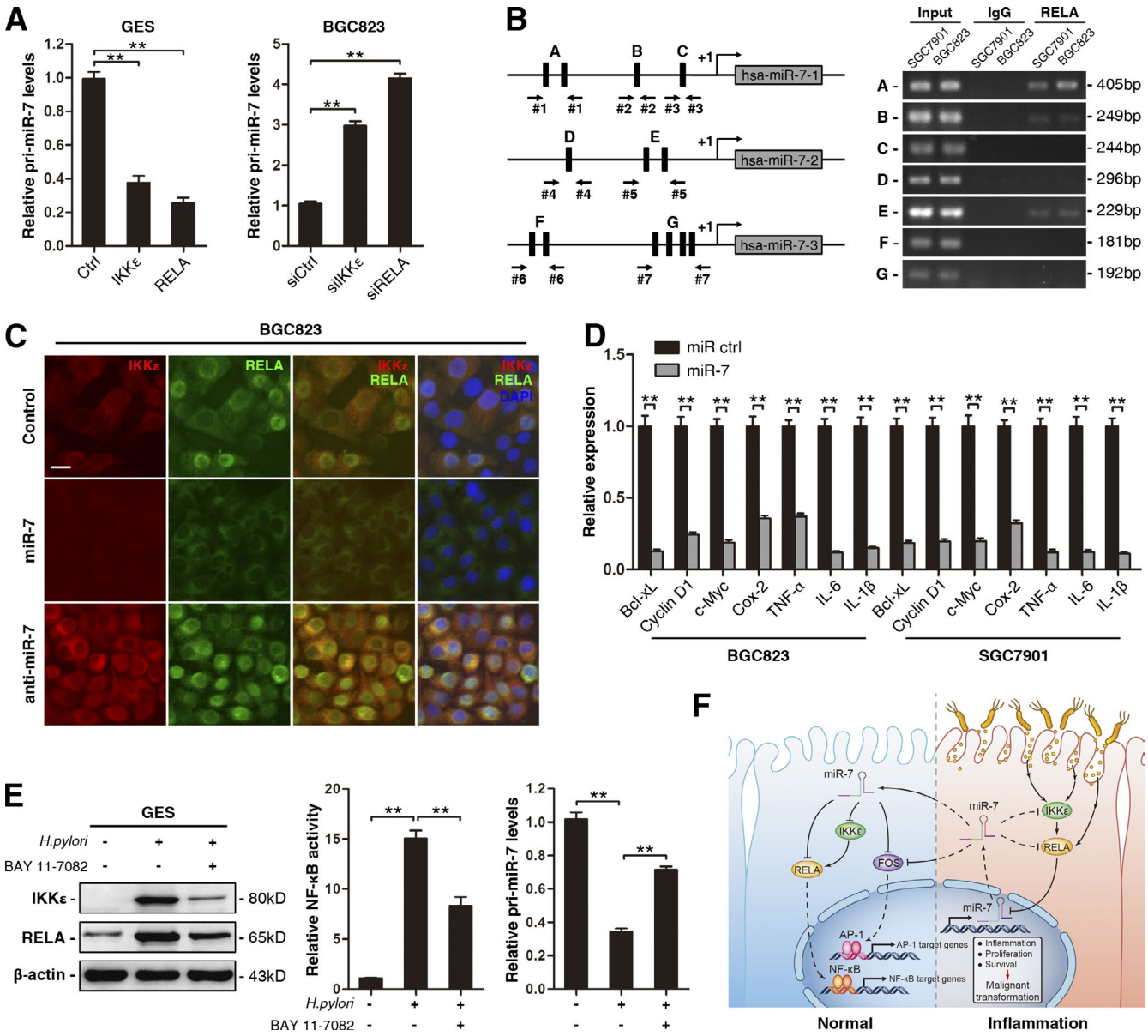

Figure 7. **miR-7 and NF-κB signaling forms a double-negative feedback loop.** (A) Real-time PCR analysis of the expression of pri-miR-7 in the indicated cells transfected with IKKε, RELA, and control (Ctrl) plasmids (left) or IKKε siRNA (siIKKε), RELA siRNA (siRELA), and control siRNA (siCtrl; right). (B, left) Schematic representation of the miR-7-1, -2, and -3 upstream promoter regions containing NF-κB binding sites. Black boxes, NF-κB binding sites; #1 to #7, PCR primer pairs for the miR-7 promoter. (right) ChIP assays revealed that RELA binds to the promoters of miR-7-1 and miR-7-2. (C) Immunofluorescence staining of IKKε and RELA after miR-7 overexpression or inhibition. Bar, 20 µm. (D) Changes in the mRNA expression of the NF-κB signaling pathway–regulated genes after miR-7 overexpression assessed by real-time PCR. (E) GES cells treated with *H. pylori* alone or together with NF-κB inhibitor BAY 11-7082 pretreatment. (left) Protein levels of IKKε and RELA were detected by Western blotting. (middle) NF-κB activity was determined with the NF-κB luciferase reporter assay. (right) Pri-miR-7 expression was assessed with real-time PCR. (F) Schematic representation of the miR-7/IKKε/RELA regulatory circuit in human gastric cells. Histograms show the means ± SD (error bars) of three experiments performed in triplicates. **, $P < 0.01$.

inhibits GC cell proliferation and induces apoptosis and cell cycle arrest, and the stable expression of miR-7 suppresses the in vivo tumorigenicity of GC cells. Second, we observed that miR-7 was reduced in almost all GC tissues compared with normal tissues, and a low expression of miR-7 in GC patients was associated with advanced TNM stage and shorter survival compared with higher miR-7 levels in our cohorts. These observations suggest that miR-7 might be a potential therapeutic target and prognostic biomarker for GC.

With respect to the mechanism, we identified *RELA* and *FOS* as direct targets of miR-7 and demonstrated that the suppression of *RELA* and *FOS* mediated the biological effects of miR-7 on gastric carcinogenesis. Our results showed that miR-7 bound to the complementary sites of the 3′-UTR of both *RELA* and *FOS* and decreased their mRNA and protein expression. Clinical data also confirmed that miR-7 expression was inversely associated with RELA or FOS levels. Furthermore, the nontargetable RELA and FOS rescued the miR-7–mediated suppression of GC cell proliferation and survival, suggesting that the inhibition of these TF family members contributes to the suppressive effects of miR-7. Our results support the notion that miRNA-induced regulatory effects can be propagated via

TFs. It has been reported that miR-504 negatively regulates p53 protein levels and impairs p53 function by binding to its 3′-UTR (Hu et al., 2010). In addition, the miR-200 family was found to regulate the cancerous epithelial–mesenchymal transition by targeting the E-box–binding TFs ZEB1 and ZEB2 (Gregory et al., 2008; Park et al., 2008). Such an miRNA-induced TF repression pattern might produce a switch-like effect to eliminate the expression of downstream TF targets with speed and reversibility (Hobert, 2008), providing an advantage over fine-tuning the expression levels of single genes and playing important roles in cellular regulatory networks.

The activation of NF-κB is essential for regulating various aspects of innate and adaptive immune responses. However, sustained and constitutive NF-κB activation can lead to tissue damage and deleterious diseases, including cancer (Staudt, 2010). Therefore, activated NF-κB must be down-modulated and properly terminated, and distinct negative regulatory mechanisms have evolved to maintain tissue homeostasis (Ruland, 2011). For example, canonical NF-κB activation induces the down-regulation of its own activity by directly regulating the genes that encode the IκB proteins. Additionally, the direct ubiquitination and degradation of IKK by deubiquitinase is another means by which NF-κB can be turned off (Ruland, 2011). In the present study, in addition to the aforementioned findings that RELA expression is directly regulated by miR-7, we found that miR-7 fine-tunes RELA activation by targeting IKKε. IKKε is an inducible IKK family member and it has been associated with the initiation and progression of multiple cancers and might function as an oncogene for malignant transformation (Verhelst et al., 2013). Our results showed that miR-7 overexpression inhibits the augmented IKKε expression and subsequently decreases RELA activation in gastric cells. This effect can be attributed to several mechanisms (Verhelst et al., 2013). One is that the down-regulation of IKKε by miR-7 decreased the phosphorylation and degradation of IκBα, which blocked RELA activation. Another explanation might be that miR-7 targeting leads to the reduced participation of IKKε in the direct phosphorylation of RELA. Other mediating molecules, however, may also contribute to the inhibitory effect of miR-7 on RELA activation, which remains to be further investigated.

In addition to the negative regulation of IKKε and RELA by miR-7, we found a reciprocal negative regulation between miR-7 and IKKε/RELA in gastric cells. This model is supported by our findings that pri-miR-7 expression is suppressed by IKKε and RELA overexpression and is rescued by IKKε and RELA knockdown. Moreover, several conserved DNA binding clusters were found upstream of the miR-7 coding sequences, and ChIP assays confirmed that RELA binds to miR-7 promoters. This miR-7/IKKε/RELA feedback loop may represent an example of a bistable system. Through this reciprocal feedback, each gene logically exerts positive feedback on itself, which correlates with the cell changing from an unstimulated state to an anti-inflammatory state. However, this feedback loop appears to be vulnerable to chronic environmental stress. Among the environmental stimuli, *H. pylori* infection is considered to be a crucial event associated with the risk of GC development and usually causes aberrant NF-κB activation (Maeda et al., 2000; Polk and Peek, 2010). Our results showed that *H. pylori* infection induces IKKε expression and increases RELA activation in gastric cells, which in turn represses miR-7 expression and leads to an imbalance in the miR-7/IKKε/RELA feedback loop. The NF-κB signaling might be permanently active through the feed-forward nature of this loop if chronic *H. pylori* infection persists, finally driving malignant transformation in gastric cells (Fig. 7 F).

In summary, this study investigated the potential role and functional mechanisms of miR-7 in GC. Based on our findings, the capability of miR-7 to control RELA and FOS may lead to the inhibition of GC progression. Our findings revealed a novel miR-7/NF-κB signaling regulatory circuit in gastric cells, implying that it may represent a new mechanism of gastric carcinogenesis and hold promise for the development of potential therapeutics against GC.

Materials and methods

Human tissue collection

Paired samples of primary GC tissues and adjacent normal tissues were obtained from patients who had undergone GC surgery at Xijing Hospital of Digestive Diseases. All samples were clinically and pathologically shown to be correctly labeled. This study was approved by Xijing Hospital's Protection of Human Subjects Committee. Informed consent was obtained from each patient.

Cell and bacterial culture

Human GC cell lines BGC823, SGC7901, AGS, MKN28, MKN45, GC9811, and SGC7901/VCR and normal gastric epithelial cell line GES were cultured in RPMI-1640 medium (HyClone) with L-glutamine, 10% fetal calf serum, and 1% penicillin-streptomycin. *H. pylori* strain 26695 was inoculated onto chocolate agar plates (BD) at 37°C under microaerophilic conditions using an anaerobic chamber (BD). Before *H. pylori* infection, GES cells seeded in 10-cm dishes were cultured to reach 80% confluency and washed twice with fresh cell culture medium containing no antibiotics. *H. pylori* was harvested, washed with PBS, and then resuspended into antibiotic-free cell culture medium. *H. pylori* was then added to GES cells at a multiplicity of infection of 100:1 and incubated for 24 h. The NF-κB inhibitor BAY 11-7082 (Santa Cruz Biotechnology, Inc.) was dissolved in DMSO (Sigma-Aldrich) and added to the cells 30 min before infection.

Mice

Female BALB/c nude mice were provided by the Experimental Animal Center of the Fourth Military Medical University. All animals were housed and maintained in pathogen-free conditions. All animal studies complied with the Fourth Military Medical University animal use guidelines, and the protocol was approved by the Fourth Military Medical University Animal Care Committee.

Constructs, oligonucleotides, and reagents

Expression vectors encoding RELA, FOS, and IKBKE were constructed by cloning the open reading frames and downstream 3′-UTRs into the pcDNA 3.1 vector (Invitrogen) between HindIII and EcoRI sites for expression driven by the CMV promoter. The 3′-UTR fragments of RELA, FOS, and IKBKE containing miR-7 putative target sites were amplified and cloned between XhoI and NotI sites downstream of the SV40 promoter-driven *Renilla* luciferase cassette in psiCHECK-2 (Promega). A site-directed mutagenesis kit (Agilent Technologies) was used to mutate the miR-7 binding sites of these vectors according to the manufacturer's instructions. An NF-κB reporter plasmid (pGL4.32 plasmid) that contains the SV40 promoter was purchased from Promega. The miR-7-5p (LV-miR-7) and shRNA-miR-7-5p (LV-anti-7) sequences were amplified and cloned into the pGC-FU vector (GeneChem) between XhoI and BamHI sites for expression driven by

the CMV promoter. Virus packaging was performed in HEK 293T cells after cotransfection using Lipofectamine 2000 (Invitrogen) of lentiviral vectors with the packaging plasmid pHelper 1.0 vector (GeneChem) and the envelope plasmid pHelper 2.0 vector (GeneChem). At 48 h after transfection, supernatants containing lentiviral particles were collected, and the virus titer was quantified according to the manufacturer's instructions. Synthetic miR-7 mimic, miR-7 inhibitor, and their negative control oligonucleotides were purchased from Ambion. siRNAs against RELA, FOS, IKBKE, and their scrambled controls were purchased from GenePharma. 1 µg/ml lipopolysaccharide (Sigma-Aldrich) was used to induce inflammation response in gastric cells. All primer and siRNA sequences used in this study are listed in Table S6.

Cell transfection and transduction

All of the constructs and oligonucleotides were transfected into indicated cells using Lipofectamine 2000 according to the manufacturer's instructions. To generate the stable cell line, BGC823 cells were infected with lentiviruses at a multiplicity of infection of 100:1. Infection efficiency was confirmed by real-time PCR 72 h after infection, and the cells were selected with 2 µg/ml puromycin for 2 wk.

RNA extraction and real-time PCR

Total RNA was extracted from cultured cells or freshly iced GC tissues with TRIzol Reagent (Invitrogen) and purified using the miRNAeasy kit (QIAGEN). The quality of RNA was examined by A260 absorption. For miRNA detection, 10 ng of total RNA was reverse transcribed into complementary DNA by using the TaqMan miRNA reverse transcription kit (Applied Biosystems). Real-time PCR was performed in triplicate with the use of the TaqMan fast advanced master mix (Applied Biosystems) on the StepOnePlus System (Applied Biosystems). The primers specific to mature and primary miR-7 were purchased from Applied Biosystems. For mRNA detection, 1 µg of total RNA was used for complementary DNA synthesis with the QuantiTect reverse transcription kit (QIAGEN). Real-time PCR was performed in triplicate using SYBR Premix Ex Taq (Takara Bio Inc.). The primers for the genes of interest were synthesized by GenePharma. The U6 small nuclear RNA and GAPDH were used, respectively, as internal control for miRNA and mRNA assays. The $2^{-\Delta\Delta CT}$ method was used to determine fold changes in the RNA levels of each sample compared with the reference sample.

Protein extraction and iTRAQ mass spectrometry analysis

BGC823 cells were seeded in 10-cm dishes and transfected with 20 nM of miR-7 mimic or control mimic. The cells were harvested after 48 h of incubation and lysed in complete lysis kit (Roche) with protease and phosphatase. Each sample (100 mg of protein) was digested with trypsin solution and labeled with the iTRAQ reagents (Applied Biosystems) with 113, 114, 115, or 116 reporter ions according to the manufacturer's protocol. Subsequently, the labeled peptides were mixed equally and separated by 1260 Infinity HPLC (Agilent Technologies), followed by nano liquid chromatography tandem mass spectrometry using the Hybrid Quadrupole-Orbitrap mass spectrometer (Q-Exactive; Thermo Fisher Scientific) equipped with a nano-UPLC RSLC Ultimate 3000 (Dionex). Both peptide identification and quantitation were performed in an overall workflow in Proteome Discoverer software (version 1.4; Thermo Fisher Scientific) and searched against the UniProt human canonical sequence protein database (October 7, 2011; 56,869 entries) using Mascot search engine (version 2.4). For protein identification, 95% confidence was used. For quantitation and further validation experiments, all reported data were based on 95% confidence for protein identification as determined by Proteome Discoverer (Unique peptide >1).

Agilent cDNA microarray analysis

BGC823 cells were seeded in 6-well plates and transfected with 20 nM miR-7 mimic or control mimic. For the microarray experiment, the 24-h time point was selected to harvest the cells to detect the more rapidly occurring changes at the mRNA level and to avoid indirect changes occurring at later time points. For Agilent gene expression profiling, 400 ng of total RNA was amplified and labeled using the Low Input Quick Amp Labeling kit (Agilent Technologies) and hybridized onto Agilent Whole Human Genome Oligonucleotides Microarrays. Preprocessing and normalization of data were performed by the Quantile algorithm in Gene Spring Software 11.0 (Agilent Technologies).

Luciferase reporter assay

For the NF-κB reporter assays, GES cells cultured in 24-well plates were transfected with reporter plasmids using Lipofectamine 2000 followed by *H. pylori* infection alone or together with BAY 11-7082 pretreatment. Cells were harvested and lysed 48 h after transfection. Luciferase assays were performed using a Dual-Luciferase Reporter Assay System (Promega) according to the manufacturer's protocol. Firefly luciferase activity normalized to *Renilla* luciferase was used as an internal control. The transfection experiments were performed in triplicate for each plasmid construct. For 3′-UTR reporter assays, BGC823 cells cultured in 24-well plates were cotransfected with miR-7 mimic, miR-7 inhibitor, or their negative controls and indicated psiCHECK-2 plasmids using Lipofectamine 2000. 48 h after transfection, *Renilla* and firefly luciferase activities were measured and the luciferase score was calculated. At least three independent transfection experiments were performed for each condition.

Western blotting

Protein lysates were separated by SDS-PAGE and transferred onto nitrocellulose membranes. After being blocked with primary and secondary HRP-conjugated antibodies in 5% nonfat milk or bovine serum albumin, immunoreactive proteins were detected with enhanced chemiluminescence reagents (Thermo Fisher Scientific). Blots were scanned by Molecular Imager ChemiDox XRS+ Imaging System with Image Lab software (Bio-Rad Laboratories). The following antibodies were used: rabbit anti–human RELA, rabbit anti–human FOS, rabbit anti–human p-RELA, mouse anti–human IκBα, rabbit anti–human p-IκBα, and mouse anti–human IKKα (Cell Signaling Technology); mouse anti–human IKKε, mouse anti–human PCNA, and mouse anti–human cyclin D1 (Santa Cruz Biotechnology, Inc.); mouse anti–human β-actin (Sigma-Aldrich); and goat anti–rabbit or goat anti–mouse IgG (Jackson ImmunoResearch Laboratories, Inc.). Densitometry of specific Western blot bands was analyzed using ImageJ version 1.48 software (National Institutes of Health) and the intensity values were normalized against the β-actin loading control. Experiments were repeated independently at least three times.

IHC and ISH

IHC for the target molecules was performed on tissue microarray chips (Shanghai Outdo Biotechnology) and single serial sections made from xenograft tumor samples. The slides were probed with the following primary antibodies: rabbit anti–human RELA (Cell Signaling Technology), rabbit anti–human FOS (Cell Signaling Technology), mouse anti–human Ki67 (Dako), and mouse anti–human PCNA (Santa Cruz Biotechnology, Inc.). Then the slides were incubated with HRP-conjugated goat anti–rabbit or goat anti–mouse secondary antibodies (Dako). The proteins were visualized in situ with DAB chromogenic substrate (Dako). ISH was performed using a 5′- and 3′-digoxigenin (DIG)–labeled locked nucleic acid–based probe specific for miR-7 (Exiqon). The probe was detected using

DIG antibody (Abcam), LSAB2 System HRP, and liquid DAB Substrate Chromogen System (Dako).

The results of IHC and ISH were independently scored by two independent observers. Ki67 and PCNA staining was quantified by counting positively stained nuclei per 400× field. A total of five random fields were scored per tumor sample and the means of these scores were calculated for further statistical analysis. miR-7, RELA, and FOS staining was quantified based on the intensity and extent of staining and was evaluated according to the following histological scoring method. The mean proportion of staining cells per specimen was determined semiquantitatively and scored as follows: 0, no positive tumor cells; 1, <10%; 2, 10–50%; and 3, >50%. The intensity of staining was determined as follows: 0, no staining; 1, weak staining; 2, moderate staining; and 3, strong staining. The staining index (SI) for each specimen was calculated as the product of staining intensity times the percentage of positive tumor cells. Using this method of assessment, we evaluated the expression of the molecule of interest in GC samples by determining the SI, with possible scores of 0, 1, 2, 3, 4, 6, and 9. Samples with an SI ≥4 were determined as having high expression, and samples with an SI <4 were determined as having low expression. Cutoff values were determined based on a measure of heterogeneity using the log-rank test with respect to overall survival. Tissue slides and tissue microarrays were scanned at room temperature using a virtual microscopy slide scanning system (VS120; Olympus) equipped with a 20×/0.75 NA objective lens (Olympus) and VS-ASW software (version 2.4; Olympus). No imaging medium was used. The IHC and ISH images were viewed using OlyVIA software (version 2.4; Olympus) and then cropped and contrast adjusted using Photoshop (CS3; Adobe).

Cell proliferation assay

BGC823 and SGC7901 cells were seeded in 6-well plates at of 2×10^5 cells per well. After incubating for 24 h, the cells were transfected with the indicated constructs or oligonucleotides. 48 h after transfection, the cells were harvested and the viable cells were seeded at a density of 3×10^3 each well onto 48-well plates. Cell proliferation was measured using methylthiazolyl blue tetrazolium bromide (Sigma-Aldrich) colorimetric dye assay in triplicate. At each time point, the cells were incubated with methylthiazolyl blue tetrazolium bromide dye for a 2–4-h incubation period at 37°C. The formazan crystals were dissolved by adding 150 µl DMSO, and the absorbance rates were read at 570 nm by a multimode microplate reader (Thermo Fisher Scientific).

Cell cycle and apoptosis assay

For cell cycle analysis, cells were seeded in 6-well plates at 2×10^5 per well. 48 after transfection, the cells were subjected to trypsin treatment and fixed in 70% ethanol at 4°C for 24 h and stained with 50 µg/ml propidium iodide (BD). The cell cycle distribution was analyzed using the fluorescence-activated cell sorter FACSCanto (BD). For apoptosis assays, cells were harvested and resuspended in staining buffer and examined using an Annexin V–FITC apoptosis detection kit (BD). Cells staining positive for Annexin V–FITC and negative for propidium iodide at 48 h after transfection were considered to have undergone apoptosis. The data were analyzed using the CellQuest Pro software (BD). The apoptotic rates of 7901/VCR cells treated with 20 µg/ml cisplatin (Sigma-Aldrich) or 50 µg/ml 5-fluorouracil (Sigma-Aldrich) for 24 h were measured by flow cytometry.

Colony formation and soft agar assay

For colony formation assays, cells were trypsinized into a single-cell suspension and seeded in 6-well plates at 10^3 per well. After 10 d of incubation, the colonies were stained with crystal violet dye. For soft agar assays, 5×10^3 cells were suspended in media containing 0.33% Select agar (Invitrogen) and plated on a bottom layer of media containing 0.5% Select agar in a 12-well plate. The cells were cultured for 2 wk before counting. All colonies were counted with a GelCount colony counter (Oxford Optronix Inc.). Images of colonies were captured at room temperature using an Advanced Microscopy Group microscope (EVOS) equipped with a 4×/0.13 NA objective lens and Micron 2.0 software (EVOS). No imaging medium was used. The images were cropped and contrast adjusted using Photoshop.

In vivo tumorigenicity assay

Lentiviral-transduced BGC823 cells (10^7 cells in 200 µl of PBS) were injected subcutaneously into each flank of 6- to 8-wk-old BALB/c nu/nu female mice (five mice per group). The tumor growth rate was monitored by measuring tumor diameters every 3 d. Both the maximum (L) and minimum (W) length of the tumor were measured using a slide caliper, and the tumor volume was calculated using the formula $V = 1/2(L \times W^2)$. The mice were killed 30 d after injection, and tumors were collected and weighed.

Northern blotting

5 µg of total RNA was fractionated on 12% denaturing polyacrylamide gel. After electrophoresis, a semi-dry transfer apparatus was used to transfer the RNA to a Hybond-N^+ nylon membrane (GE Healthcare). The RNA was then fixed by UV cross-linking according to the manufacturer's instructions. The membrane was prehybridized with ULTRAhyb buffer (Ambion) for 1 h and then probed overnight with specific 3′-DIG–labeled locked nucleic acid oligonucleotides for mature miR-7 or U6 small nuclear RNA (Exiqon). Detection was performed with an antibody to 3′-DIG (Roche). Northern blot analyses were conducted in biological triplicate.

ChIP assay

ChIP assays were performed using the Magna ChIP G Assay kit (EMD Millipore). Cells were cross-linked with 1% formaldehyde for 10 min at room temperature and quenched in glycine. DNA was immunoprecipitated from the sonicated cell lysates using a rabbit anti–human RELA antibody (Cell Signaling Technology) and subjected to PCR to amplify the NF-κB binding sites. The amplified fragments were then analyzed using agarose gel. 10% of chromatin before immunoprecipitation was used as the input control, and a nonspecific antibody against IgG (BD) served as the negative control.

Immunofluorescence

Cells were plated onto glass coverslips and fixed with 4% paraformaldehyde for 20 min and permeabilized with 0.1% Triton X-100 in PBS for 15 min. Blocking solution was applied for 1 h at room temperature. Primary antibodies, mouse anti–human IKKε (Santa Cruz Biotechnology, Inc.) and rabbit anti–human RELA (Cell Signaling Technology, Inc.), were applied at 4°C overnight. FITC-conjugated goat anti–rabbit and Cy3-conjugated goat anti–mouse secondary antibodies were loaded and incubated for 2 h at room temperature. Immunostaining signals and DAPI-stained nuclei were visualized at room temperature using a confocal microscope (FV10i; Olympus) equipped with a 10×/0.30 NA objective lens (Olympus) and Fluoview software (version 4.3; Olympus). No imaging medium was used. For better visualization, the images were adjusted using the levels and brightness/contrast tools in Photoshop according to the guidelines for the presentation of digital data.

Statistical analysis

All statistical data were analyzed with the Statistical Program for Social Sciences 17.0 software (SPSS). Normally distributed data are presented as the mean ± SD. Differences between means were assessed using Stu-

dent's *t* test or one-way analysis of variance. Frequencies of categorical variables were compared using the χ^2 test. Spearman's rank correlation coefficients were computed for assessing mutual association among clinical results. $P < 0.05$ was considered to be statistically significant.

Online supplemental material

Fig. S1 shows the transfection efficiency of an miR-7 mimic in BGC823 cells. Fig. S2 shows the relative luciferase activity levels in BGC823 cells cotransfected with miR-7 inhibitor or miRNA inhibitor negative control and wild-type or mutant *RELA* and *FOS* 3′-UTR vectors. Fig. S3 shows the efficiency of knockdown and overexpression of RELA and FOS and their effects on the growth of SGC7901 cells. Fig. S4 shows that miR-7 inhibits GC cell growth in vivo and regulates RELA activation by modulating IKKε. Fig. S5 shows the knockdown effects of IKKε siRNAs on the protein levels of IKKε in GC cells and the expression of mature miR-7 after modulating IKKε and RELA expression. Table S1 and S2 shows the transcripts and proteins significantly down-regulated by miR-7 overexpression in BGC823 cells. Table S3 shows 39 genes reduced at both protein and RNA levels by miR-7 overexpression in BGC823 cells. Tables S4 and S5 show the transcripts and proteins significantly up-regulated by miR-7 overexpression in BGC823 cells. Table S6 contain the information of primers used for 3′-UTR mutagenesis, real-time PCR, and ChIP assays and oligonucleotides used for RNA interference. Online supplemental material is available at http://www.jcb.org/cgi/content/full/jcb.201501073/DC1.

Acknowledgments

We acknowledge Robert J. Coffey and Fernando D. Camargo for their generous help to this study. We also grateful to Zeng Li, Ming Bai, Miao-Miao Tian, and Zu-Hong Tian for their technical assistance.

This work was supported by grants from the National Basic Research Program of China (973 Program, No. 2010CB529300), the National Natural Science Foundation of China (No. 81430072, 81120108005, 81225003, 81470805, 81270445, 81201929, 30900675, and 81372609), the Ministry of Science and Technology of China (No. 2012AA02A504 and 2015BAI13B07), and the China Scholarship Council (No. 201306590015).

The authors declare no competing financial interests.

Submitted: 19 January 2015
Accepted: 30 June 2015

References

Bartel, D.P. 2004. MicroRNAs: genomics, biogenesis, mechanism, and function. *Cell.* 116:281–297. http://dx.doi.org/10.1016/S0092-8674(04)00045-5

Cancer Genome Atlas Research Network. 2014. Comprehensive molecular characterization of gastric adenocarcinoma. *Nature.* 513:202–209. http://dx.doi.org/10.1038/nature13480

Chou, Y.T., H.H. Lin, Y.C. Lien, Y.H. Wang, C.F. Hong, Y.R. Kao, S.C. Lin, Y.C. Chang, S.Y. Lin, S.J. Chen, et al. 2010. EGFR promotes lung tumorigenesis by activating miR-7 through a Ras/ERK/Myc pathway that targets the Ets2 transcriptional repressor ERF. *Cancer Res.* 70:8822–8831. http://dx.doi.org/10.1158/0008-5472.CAN-10-0638

Clément, J.F., S. Meloche, and M.J. Servant. 2008. The IKK-related kinases: from innate immunity to oncogenesis. *Cell Res.* 18:889–899. http://dx.doi.org/10.1038/cr.2008.273

Correa, P. 1992. Human gastric carcinogenesis: a multistep and multifactorial process—First American Cancer Society Award Lecture on Cancer Epidemiology and Prevention. *Cancer Res.* 52:6735–6740.

Ding, S.Z., J.B. Goldberg, and M. Hatakeyama. 2010. *Helicobacter pylori* infection, oncogenic pathways and epigenetic mechanisms in gastric carcinogenesis. *Future Oncol.* 6:851–862. http://dx.doi.org/10.2217/fon.10.37

Eferl, R., and E.F. Wagner. 2003. AP-1: a double-edged sword in tumorigenesis. *Nat. Rev. Cancer.* 3:859–868. http://dx.doi.org/10.1038/nrc1209

Esquela-Kerscher, A., and F.J. Slack. 2006. Oncomirs — microRNAs with a role in cancer. *Nat. Rev. Cancer.* 6:259–269. http://dx.doi.org/10.1038/nrc1840

Fang, Y., J.L. Xue, Q. Shen, J. Chen, and L. Tian. 2012. MicroRNA-7 inhibits tumor growth and metastasis by targeting the phosphoinositide 3-kinase/Akt pathway in hepatocellular carcinoma. *Hepatology.* 55:1852–1862. http://dx.doi.org/10.1002/hep.25576

Fearon, E.R., and B. Vogelstein. 1990. A genetic model for colorectal tumorigenesis. *Cell.* 61:759–767. http://dx.doi.org/10.1016/0092-8674(90)90186-I

Giles, K.M., R.A. Brown, M.R. Epis, F.C. Kalinowski, and P.J. Leedman. 2013. miRNA-7-5p inhibits melanoma cell migration and invasion. *Biochem. Biophys. Res. Commun.* 430:706–710. http://dx.doi.org/10.1016/j.bbrc.2012.11.086

Gregory, P.A., A.G. Bert, E.L. Paterson, S.C. Barry, A. Tsykin, G. Farshid, M.A. Vadas, Y. Khew-Goodall, and G.J. Goodall. 2008. The miR-200 family and miR-205 regulate epithelial to mesenchymal transition by targeting ZEB1 and SIP1. *Nat. Cell Biol.* 10:593–601. http://dx.doi.org/10.1038/ncb1722

Hanahan, D., and R.A. Weinberg. 2011. Hallmarks of cancer: the next generation. *Cell.* 144:646–674. http://dx.doi.org/10.1016/j.cell.2011.02.013

He, L., and G.J. Hannon. 2004. MicroRNAs: small RNAs with a big role in gene regulation. *Nat. Rev. Genet.* 5:522–531. http://dx.doi.org/10.1038/nrg1379

Herrera, V., and J. Parsonnet. 2009. *Helicobacter pylori* and gastric adenocarcinoma. *Clin. Microbiol. Infect.* 15:971–976. http://dx.doi.org/10.1111/j.1469-0691.2009.03031.x

Hobert, O. 2008. Gene regulation by transcription factors and microRNAs. *Science.* 319:1785–1786. http://dx.doi.org/10.1126/science.1151651

Hu, W., C.S. Chan, R. Wu, C. Zhang, Y. Sun, J.S. Song, L.H. Tang, A.J. Levine, and Z. Feng. 2010. Negative regulation of tumor suppressor p53 by microRNA miR-504. *Mol. Cell.* 38:689–699. http://dx.doi.org/10.1016/j.molcel.2010.05.027

Jiang, L., X. Liu, Z. Chen, Y. Jin, C.E. Heidbreder, A. Kolokythas, A. Wang, Y. Dai, and X. Zhou. 2010. MicroRNA-7 targets IGF1R (insulin-like growth factor 1 receptor) in tongue squamous cell carcinoma cells. *Biochem. J.* 432:199–205. http://dx.doi.org/10.1042/BJ20100859

Kalinowski, F.C., K.M. Giles, P.A. Candy, A. Ali, C. Ganda, M.R. Epis, R.J. Webster, and P.J. Leedman. 2012. Regulation of epidermal growth factor receptor signaling and erlotinib sensitivity in head and neck cancer cells by miR-7. *PLoS ONE.* 7:e47067. http://dx.doi.org/10.1371/journal.pone.0047067

Kalinowski, F.C., R.A. Brown, C. Ganda, K.M. Giles, M.R. Epis, J. Horsham, and P.J. Leedman. 2014. microRNA-7: a tumor suppressor miRNA with therapeutic potential. *Int. J. Biochem. Cell Biol.* 54:312–317. http://dx.doi.org/10.1016/j.biocel.2014.05.040

Karin, M., and F.R. Greten. 2005. NF-κB: linking inflammation and immunity to cancer development and progression. *Nat. Rev. Immunol.* 5:749–759. http://dx.doi.org/10.1038/nri1703

Kefas, B., J. Godlewski, L. Comeau, Y. Li, R. Abounader, M. Hawkinson, J. Lee, H. Fine, E.A. Chiocca, S. Lawler, and B. Purow. 2008. microRNA-7 inhibits the epidermal growth factor receptor and the Akt pathway and is down-regulated in glioblastoma. *Cancer Res.* 68:3566–3572. http://dx.doi.org/10.1158/0008-5472.CAN-07-6639

Kong, D., Y.S. Piao, S. Yamashita, H. Oshima, K. Oguma, S. Fushida, T. Fujimura, T. Minamoto, H. Seno, Y. Yamada, et al. 2012. Inflammation-induced repression of tumor suppressor miR-7 in gastric tumor cells. *Oncogene.* 31:3949–3960. http://dx.doi.org/10.1038/onc.2011.558

Li, Q., and I.M. Verma. 2002. NF-κB regulation in the immune system. *Nat. Rev. Immunol.* 2:725–734. http://dx.doi.org/10.1038/nri910

Li, C., Q. Xiong, J. Zhang, F. Ge, and L.J. Bi. 2012. Quantitative proteomic strategies for the identification of microRNA targets. *Expert Rev. Proteomics.* 9:549–559. http://dx.doi.org/10.1586/epr.12.49

Li, Y., Y. Li, Y. Liu, P. Xie, F. Li, and G. Li. 2014. PAX6, a novel target of microRNA-7, promotes cellular proliferation and invasion in human colorectal cancer cells. *Dig. Dis. Sci.* 59:598–606. http://dx.doi.org/10.1007/s10620-013-2929-x

Liu, S., P. Zhang, Z. Chen, M. Liu, X. Li, and H. Tang. 2013. MicroRNA-7 downregulates XIAP expression to suppress cell growth and promote apoptosis in cervical cancer cells. *FEBS Lett.* 587:2247–2253. http://dx.doi.org/10.1016/j.febslet.2013.05.054

Ma, J., B. Fang, F. Zeng, H. Pang, J. Zhang, Y. Shi, X. Wu, L. Cheng, C. Ma, J. Xia, and Z. Wang. 2014. Curcumin inhibits cell growth and invasion through up-regulation of miR-7 in pancreatic cancer cells. *Toxicol. Lett.* 231:82–91. http://dx.doi.org/10.1016/j.toxlet.2014.09.014

Maeda, S., H. Yoshida, K. Ogura, Y. Mitsuno, Y. Hirata, Y. Yamaji, M. Akanuma, Y. Shiratori, and M. Omata. 2000. *H. pylori* activates NF-κB through a signaling pathway involving IκB kinases, NF-κB–inducing kinase, TRAF2, and TRAF6 in gastric cancer cells. *Gastroenterology.* 119:97–108. http://dx.doi.org/10.1053/gast.2000.8540

Park, S.M., A.B. Gaur, E. Lengyel, and M.E. Peter. 2008. The miR-200 family determines the epithelial phenotype of cancer cells by targeting the E-cadherin repressors ZEB1 and ZEB2. *Genes Dev.* 22:894–907. http://dx.doi.org/10.1101/gad.1640608

Polk, D.B., and R.M. Peek Jr. 2010. *Helicobacter pylori*: gastric cancer and beyond. *Nat. Rev. Cancer.* 10:403–414. http://dx.doi.org/10.1038/nrc2857

Quante, M., J. Varga, T.C. Wang, and F.R. Greten. 2013. The gastrointestinal tumor microenvironment. *Gastroenterology.* 145:63–78. http://dx.doi.org/10.1053/j.gastro.2013.03.052

Rai, K., N. Takigawa, S. Ito, H. Kashihara, E. Ichihara, T. Yasuda, K. Shimizu, M. Tanimoto, and K. Kiura. 2011. Liposomal delivery of MicroRNA-7–expressing plasmid overcomes epidermal growth factor receptor tyrosine kinase inhibitor-resistance in lung cancer cells. *Mol. Cancer Ther.* 10:1720–1727. http://dx.doi.org/10.1158/1535-7163.MCT-11-0220

Reddy, S.D., K. Ohshiro, S.K. Rayala, and R. Kumar. 2008. MicroRNA-7, a homeobox D10 target, inhibits p21-activated kinase 1 and regulates its functions. *Cancer Res.* 68:8195–8200. http://dx.doi.org/10.1158/0008-5472.CAN-08-2103

Ruland, J. 2011. Return to homeostasis: downregulation of NF-κB responses. *Nat. Immunol.* 12:709–714. http://dx.doi.org/10.1038/ni.2055

Saydam, O., O. Senol, T. Würdinger, A. Mizrak, G.B. Ozdener, A.O. Stemmer-Rachamimov, M. Yi, R.M. Stephens, A.M. Krichevsky, N. Saydam, et al. 2011. miRNA-7 attenuation in Schwannoma tumors stimulates growth by upregulating three oncogenic signaling pathways. *Cancer Res.* 71:852–861. http://dx.doi.org/10.1158/0008-5472.CAN-10-1219

Sethupathy, P., M. Megraw, and A.G. Hatzigeorgiou. 2006. A guide through present computational approaches for the identification of mammalian microRNA targets. *Nat. Methods.* 3:881–886. http://dx.doi.org/10.1038/nmeth954

Siegel, R., J. Ma, Z. Zou, and A. Jemal. 2014. Cancer statistics, 2014. *CA Cancer J. Clin.* 64:9–29. http://dx.doi.org/10.3322/caac.21208

Siomi, H., and M.C. Siomi. 2010. Posttranscriptional regulation of microRNA biogenesis in animals. *Mol. Cell.* 38:323–332. http://dx.doi.org/10.1016/j.molcel.2010.03.013

Song, S., and J.A. Ajani. 2013. The role of microRNAs in cancers of the upper gastrointestinal tract. *Nat. Rev. Gastroenterol. Hepatol.* 10:109–118. http://dx.doi.org/10.1038/nrgastro.2012.210

Staudt, L.M. 2010. Oncogenic activation of NF-κB. *Cold Spring Harb. Perspect. Biol.* 2:a000109. http://dx.doi.org/10.1101/cshperspect.a000109

Thomas, M., J. Lieberman, and A. Lal. 2010. Desperately seeking microRNA targets. *Nat. Struct. Mol. Biol.* 17:1169–1174. http://dx.doi.org/10.1038/nsmb.1921

Verhelst, K., L. Verstrepen, I. Carpentier, and R. Beyaert. 2013. IκB kinase ε (IKKε): A therapeutic target in inflammation and cancer. *Biochem. Pharmacol.* 85:873–880. http://dx.doi.org/10.1016/j.bcp.2013.01.007

Webster, R.J., K.M. Giles, K.J. Price, P.M. Zhang, J.S. Mattick, and P.J. Leedman. 2009. Regulation of epidermal growth factor receptor signaling in human cancer cells by microRNA-7. *J. Biol. Chem.* 284:5731–5741. http://dx.doi.org/10.1074/jbc.M804280200

Xiong, S., Y. Zheng, P. Jiang, R. Liu, X. Liu, and Y. Chu. 2011. MicroRNA-7 inhibits the growth of human non-small cell lung cancer A549 cells through targeting BCL-2. *Int. J. Biol. Sci.* 7:805–814. http://dx.doi.org/10.7150/ijbs.7.805

Xu, L., Z. Wen, Y. Zhou, Z. Liu, Q. Li, G. Fei, J. Luo, and T. Ren. 2013. MicroRNA-7–regulated TLR9 signaling–enhanced growth and metastatic potential of human lung cancer cells by altering the phosphoinositide-3-kinase, regulatory subunit 3/Akt pathway. *Mol. Biol. Cell.* 24:42–55. http://dx.doi.org/10.1091/mbc.E12-07-0519

Yu, Z., L. Ni, D. Chen, Q. Zhang, Z. Su, Y. Wang, W. Yu, X. Wu, J. Ye, S. Yang, et al. 2013. Identification of miR-7 as an oncogene in renal cell carcinoma. *J. Mol. Histol.* 44:669–677. http://dx.doi.org/10.1007/s10735-013-9516-5

Zhang, N., X. Li, C.W. Wu, Y. Dong, M. Cai, M.T. Mok, H. Wang, J. Chen, S.S. Ng, M. Chen, et al. 2013. microRNA-7 is a novel inhibitor of YY1 contributing to colorectal tumorigenesis. *Oncogene.* 32:5078–5088. http://dx.doi.org/10.1038/onc.2012.526

Zhang, X., S. Hu, X. Zhang, L. Wang, X. Zhang, B. Yan, J. Zhao, A. Yang, and R. Zhang. 2014. MicroRNA-7 arrests cell cycle in G1 phase by directly targeting CCNE1 in human hepatocellular carcinoma cells. *Biochem. Biophys. Res. Commun.* 443:1078–1084. http://dx.doi.org/10.1016/j.bbrc.2013.12.095

Zhao, X., W. Dou, L. He, S. Liang, J. Tie, C. Liu, T. Li, Y. Lu, P. Mo, Y. Shi, et al. 2013. MicroRNA-7 functions as an anti-metastatic microRNA in gastric cancer by targeting insulin-like growth factor-1 receptor. *Oncogene.* 32:1363–1372. http://dx.doi.org/10.1038/onc.2012.156